Effect of annealing on the depth profile of hole concentration in (Ga,Mn)As

W. Limmer,* A. Koeder, S. Frank, V. Avrutin, W. Schoch, and R. Sauer
Abteilung Halbleiterphysik, Universität Ulm, D-89069 Ulm, Germany

K. Zuern, J. Eisenmenger, and P. Ziemann
Abteilung Festkörperphysik, Universität Ulm, D-89069 Ulm, Germany

E. Peiner and A. Waag
Institut für Halbleitertechnik, Technische Universität Braunschweig, D-38023 Braunschweig, Germany
(Received 30 June 2004; revised manuscript received 22 February 2005; published 31 May 2005)

The effect of annealing at 250 °C on the carrier depth profile, Mn distribution, electrical conductivity, and Curie temperature of (Ga,Mn)As layers with thicknesses $\geqslant$200 nm, grown by molecular-beam epitaxy at low temperatures, is studied by a variety of analytical methods. The vertical gradient in hole concentration, revealed by electrochemical capacitance-voltage profiling, is shown to play a key role in the understanding of conductivity and magnetization data. The gradient, basically already present in as-grown samples, is strongly influenced by post-growth annealing. From secondary ion mass spectroscopy it can be concluded that, at least in thick layers, the change in carrier depth profile and thus in conductivity is not primarily due to out-diffusion of Mn interstitials during annealing. Two alternative possible models are discussed.

DOI: 10.1103/PhysRevB.71.205213 PACS number(s): 75.50.Pp, 61.72.Cc, 81.40.Rs, 78.30.Fs

I. INTRODUCTION

Semiconductor-based spintronic technology, where both the electrical charge and the spin of carriers are utilized for signal processing and storage, calls for the development of new ferromagnetic materials. The III-V dilute magnetic semiconductor (Ga,Mn)As, being compatible with conventional semiconductor technology, is considered a potential candidate for spintronics and has been intensely studied during the past few years.[1–3] The ferromagnetic properties of (Ga,Mn)As, successfully explained within the Zener mean-field model,[4] arise from the $S=5/2$ spins of Mn atoms incorporated on Ga lattice sites. The ferromagnetic Mn-Mn coupling is mediated by delocalized or weakly localized holes which are supplied by the Mn atoms acting as acceptors on Ga lattice sites. The Mn spin system undergoes a ferromagnetic phase transition at the Curie temperature T_C which is suggested to strongly depend on both the Mn content and the hole concentration.[4] (Ga,Mn)As is grown by molecular-beam epitaxy (MBE) at low temperatures ($\sim$250 °C). In most cases, T_C is increased by post-growth annealing at temperatures near or even below the growth temperature, resulting in values of up to 160 K in (Ga,Mn)As single layers, as reported so far.[5–12] This is commonly explained by the removal or rearrangement of highly unstable compensating defects such as Mn atoms on interstitial lattice sites.[10–14] The enhancement of the ferromagnetism associated with low-temperature (LT) annealing is suppressed in the presence of a thin GaAs capping layer, indicating that diffusion of defects towards the surface plays a crucial role in the annealing process.[11,12] It has been revealed by electrochemical capacitance voltage (ECV) profiling and Raman spectroscopy that in general the hole concentration p is not constant throughout the (Ga,Mn)As layer but exhibits a vertical gradient.[15] Starting at the GaAs/(Ga,Mn)As interface, p monotonously increases and reaches its maximum value near the sample surface. This finding is in agreement with the results of spin-wave resonance experiments which manifest the existence of a gradient in the magnetic properties.[16,17]

For (Ga,Mn)As, it is well known that, within a limited temperature range, a slight increase of the growth temperature results in a pronounced enhancement of both T_C and p.[18] In addition, a significant increase of the surface temperature, induced by heat radiation from the effusion cells, has been detected during LT MBE growth of GaAs.[19,20] Therefore, we suppose that besides annealing effects during growth, a gradual increase of the surface temperature due do free-carrier absorption is likely to account for the observed gradient. Even though it is disregarded by most other groups so far, the presence of the gradient seems to be a general phenomenon, whereas its specific profile depends on several parameters such as sample thickness and growth conditions. From the p dependence of T_C, it becomes obvious that a pronounced variation in p along the growth direction must have a strong impact on the electrical and magnetic properties of (GaMn)As.

In this work, the effect of annealing at 250 °C on the depth profile of hole concentration in (Ga,Mn)As epilayers with thicknesses between 0.2 and 1.2 μm is studied by ECV profiling, micro-Raman spectroscopy, conductivity measurements, superconducting quantum interference device (SQUID) magnetization measurements, and secondary ion mass spectroscopy (SIMS). It is shown that the gradient in the carrier density plays a key role in the understanding of annealing-induced effects, such as the increase in conductivity and Curie temperature. From our SIMS and ECV data we infer that, at least in thick layers ($\sim$1 μm), out-diffusion of Mn interstitials is not the dominant mechanism for the annealing-induced enhancement of the hole density, as recently proposed for thin layers ($\leqslant$100 nm).[10,12] While most reports in the literature are on (Ga,Mn)As epilayers with thicknesses in the range of 10–200 nm, where the gradient is

probably less pronounced, thicker samples, as considered in this work, allow us to map the depth profiles, e.g., of the hole and Mn concentration over larger distances, and therefore to get more detailed information on the understanding of the defect dynamics. Provided that the fundamental diffusion processes during annealing are primarily independent of the layer thickness, the findings reported in this paper may be helpful in the interpretation of experimental data obtained from much thinner samples as well.

II. EXPERIMENTAL DETAILS

(Ga,Mn)As layers were grown in a RIBER 32 MBE machine on In-mounted semi-insulating VGF GaAs(001) substrates using a conventional Knudsen cell and a hot-lip effusion cell to provide the Ga and Mn fluxes, respectively. A valved arsenic cracker cell was used in the noncracking mode to supply As_4 with a maximum V/III flux ratio of about 3. First, a GaAs buffer layer around 100 nm thick was grown at a temperature of T_s=585 °C (conventional substrate temperature for GaAs), then the growth was interrupted and T_s was lowered to ~250 °C. The Mn concentrations in the 0.2–1.2-μm-thick (Ga,Mn)As layers under study were determined by flux measurements, which have been checked by elastic recoil detection measurements (ERD). For details about ERD, see Ref. 21.

ECV analyses were performed using a Bio-Rad PN4200 profiler. The electrolyte (250 mL aqueous solution of 2.0 g NaOH+9.3 g EDTA) is in contact with the semiconductor forming an electrolyte-semiconductor diode. A low-resistance Ohmic contact can be established for the (Ga,Mn)As sample without metallization. The potential of the sample is measured potentiometrically with reference to a saturated calomel electrode. The admittance Y of the electrolyte-semiconductor contact is determined by ac measurements under reverse bias at ω_c. Additionally, the bias voltage V_m is wobbled at a considerably lower modulation frequency to yield the differential admittance dY/dV. V_m and ω_c are selected to obtain optimum Schottky characteristics of the electrolyte-semiconductor contact. The corresponding equivalent circuit which is implemented in the analysis software consists of the space-charge layer capacitance C and of resistances R_p and R_s connected in parallel and in series, respectively. R_s is obtained from the admittance data measured at two different frequencies ω_c. Using Y, dY/dV, and R_s, we can determine C and dC/dV yielding the carrier concentration $N(w_d)$ at the edge of the depletion region of width w_d according to

$$N(w_d) = -\frac{C^3}{e\varepsilon A^2}\left(\frac{dC}{dV}\right)^{-1} \tag{1}$$

with

$$w_d = \frac{\varepsilon A}{C}, \tag{2}$$

where ε(0.12 nF/m) and e are the permittivity of GaAs and the electron charge, respectively. Controlled amounts of (Ga,Mn)As are removed in increments of a few tens of nanometers by passing a dc current I between the anodically polarized semiconductor and a carbon counter electrode. The removed layer thickness w_e is calculated from the accumulated transferred charge using Faraday's law of electrolysis,

$$w_e = \frac{M}{zF\rho A}\int Idt, \tag{3}$$

where M(144.6), z(6), ρ(5.36 g/cm^3), and F(96 490 As mol^{-1}) denote the molecular weight, effective dissolution valence, density of GaAs, and Faraday's constant, respectively. Additionally, w_e is controlled by mechanical surface tracing. The diode area A of 0.005–0.008 cm^2 is defined by a plastic sealing ring. Normally, A is not accurately known at the beginning of an ECV profiling run, but is routinely measured subsequently. Relevant recalculation procedures considering the measured values of A and the series resistance R_s are implemented in the original Bio-Rad software of the PN 4200 ECV profiler. The measured ECV profiles are reproducible within an uncertainty in the absolute values of about 15%. More information about ECV profiling can be found in Ref. 22.

Hole concentrations in (Ga,Mn)As can also be estimated from Raman scattering by coupled plasmon–LO-phonon modes.[23,24] Therefore, micro-Raman measurements were performed at room temperature (RT) using the 514-nm line of an Ar^+ laser as an excitation source. The Raman signals were detected in the backscattering configuration $\overline{z}(x,y)z$ using a DILOR XY 800-mm triple-grating spectrometer with a confocal entrance optics and a LN_2-cooled charge-coupled device detector. Further experimental details of the micro-Raman measurements are given in Ref. 23.

For the electrical measurements, Hall bars with Ti-AuPt-Au contacts were prepared on several pieces of the cleaved samples without annealing. The contacts were checked to be Ohmic with negligibly low resistance. The samples were annealed in air using a LINKAM THMS 600 heating chamber equipped with an electrical feed through, which enabled us to perform *in situ* measurements of the conductivity. They were mounted on a silver block which could be heated electrically or cooled by liquid nitrogen over the temperature range from −200 to 300 °C within 2 min.

To measure depth profiles of the Mn fraction, SIMS experiments were performed using a commercial Cameca ims4f-E6 spectrometer with Cs^+ as primary ion beam (net impact energy 5.5 keV) at a sputter rate of about 1 nm/s. In the absence of appropriate calibration standards for Mn, the quantitative analysis of the Mn fraction refers to the flux measurement of sample B313, which gave us a value of 6%. A detailed introduction into the SIMS measuring method is given in Ref. 25.

The magnetization measurements were carried out in a QUANTUM DESIGN MPMS 5 SQUID magnetometer applying an in-plane magnetic field of 5 mT.

III. RESULTS AND DISCUSSION

The phenomena discussed in this paper have been qualitatively observed in all (Ga,Mn)As layers grown at V/III flux

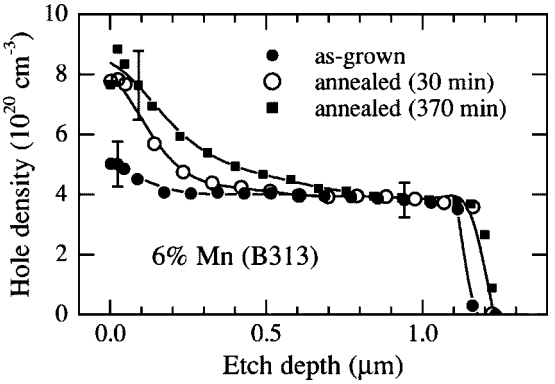

FIG. 1. ECV profiles recorded from sample B313 before and after annealing at 250 °C for 30 and 370 min.

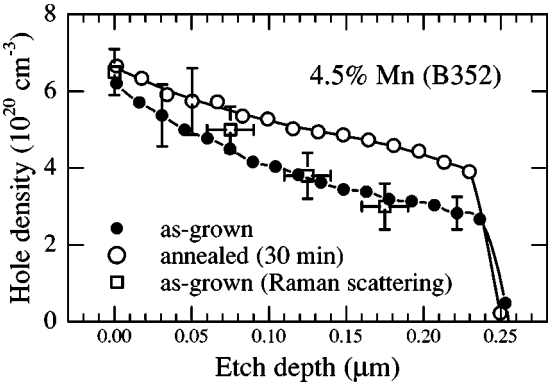

FIG. 2. ECV profiles recorded from sample B352 before and after annealing at 250 °C for 30 min. Depth-dependent hole concentrations determined from Raman spectroscopy are depicted for comparison.

ratios $\leqslant 3$, exhibiting thicknesses between 200 nm and 1.2 μm. The specific influence of the V/III flux ratio on the structural, electric, and magnetic properties of (Ga,Mn)As is not a subject of this work and will be discussed elsewhere. In the following, we present experimental results obtained from several pieces of a 1.2-μm-thick (Ga,Mn)As epilayer with a Mn fraction of 6% (sample B313) and of a 240-nm-thick epilayer with a Mn fraction of 4.5% (sample B352). These epilayers are representative for all other samples investigated so far.

As mentioned above, ECV profiling reveals the presence of a vertical gradient in the hole concentration. Figure 1 depicts the ECV profiles of sample B313 before and after annealing at 250 °C for 30 and 370 min. It is clearly seen that the gradient, already present in the as-grown sample, is strongly enhanced by post-growth annealing, leading to a hole density near the sample surface which is almost twice as high as near the GaAs/(Ga,Mn)As interface. As a consequence, the electric and magnetic properties of the (Ga,Mn)As layer are affected in a dramatic way, as will be shown below. Whereas the total hole concentration, averaged over the layer thickness, increases from $(3.8\pm0.6)\times10^{20}$ cm^{-3} in the as-grown sample to $(4.3\pm0.6)\times10^{20}$ cm^{-3} in the 30-min-annealed sample and to $(4.9\pm0.7)\times10^{20}$ cm^{-3} in the 370-min-annealed sample, the local hole density near the sample surface almost saturates after annealing for 30 min. The particular evolution of the carrier depth profile in the course of the annealing seems to corroborate the assumption that out-diffusion of compensating defects towards the surface accounts for the increase in hole density during post-growth annealing.[10–12]

The ECV profiles of sample B352, recorded before and after annealing at 250 °C for 30 min, are shown in Fig. 2. The gradient in the as-grown sample is much more pronounced than in B313 and flattens upon annealing with a concomitant increase in the total hole concentration. The ECV profiles resemble those of sample B313 in the range from the surface down to ~240 nm after annealing for 30 and 370 min.

In order to make sure that ECV profiles reflect the correct depth distribution of the hole concentration, confirmative optical experiments were performed. To this end, steplike surface profiles with flat terraces at different depths below the initial surface were prepared on several (Ga,Mn)As layers by wet chemical etching. Micro-Raman spectra were taken from each of the individual terraces, and the carrier densities, obtained from a line-shape analysis of the Raman signals, were compared with the ECV data. Figure 2 shows, as an example, such a comparison for the as-grown sample B352. Within the error margin of the two-analysis methods, the measured depth profiles coincide almost perfectly.

The Raman spectra corresponding to the data points in Fig. 2 are depicted in Fig. 3. The high hole concentration in (Ga,Mn)As leads to the formation of a phononlike coupled mode of the longitudinal-optical (LO) phonon and the overdamped hole plasmon.[26] With increasing hole concentration, this mode shifts from the frequency of the LO phonon to that of the transverse-optical (TO) phonon. It is clearly seen in Fig. 3 that the coupled mode broadens and shifts to higher frequencies with increasing etch depth, indicating a decrease in the hole concentration. At an etch depth of 175 nm, the remaining layer thickness nearly matches the information depth of $1/2\alpha\approx50$ nm of the Raman measurement, where α denotes the absorption coefficient at a 514 nm wavelength of the Ar^+ laser. Therefore, the narrow Raman line of the pure

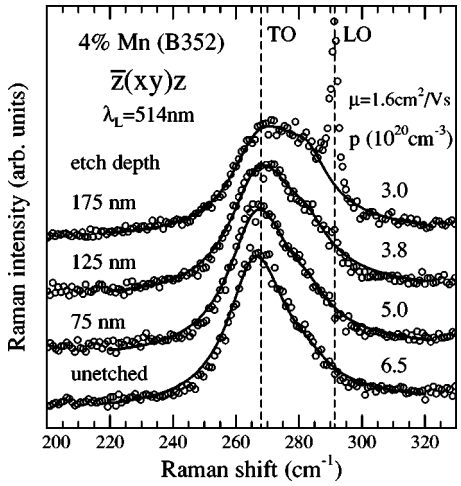

FIG. 3. Raman spectra recorded from sample B352 for different etch depths.

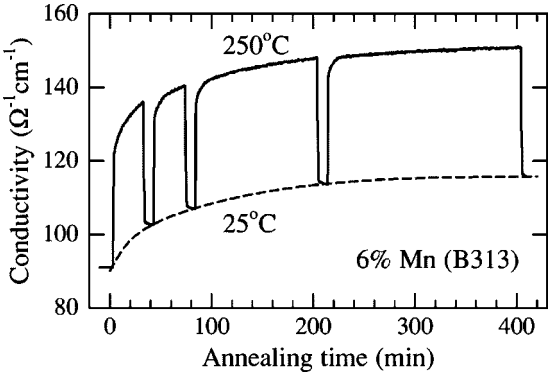

FIG. 4. *In situ* monitoring of the conductivity of sample B313 during annealing at 250 °C.

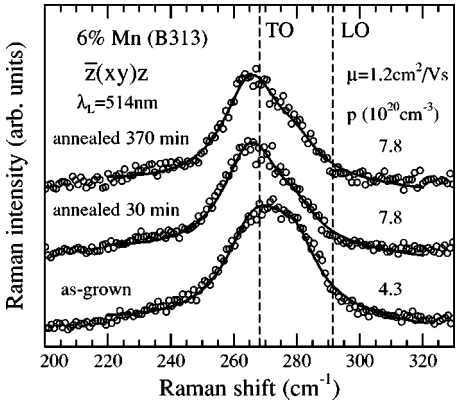

FIG. 5. Raman spectra recorded from sample B313 before and after annealing at 250 °C. The solid lines are calculated line shapes.

LO-phonon mode in the undoped substrate appears at 292 cm^{-1}. The values for the hole densities were obtained from line-shape analyses of the Raman spectra using a value for the hole mobility of 1.6 cm^2/Vs. The calculated line shapes are drawn as solid lines in Fig. 3. Details concerning the calculation of Raman line shapes in heavily *p*-doped semiconductors can be found in Refs. 23 and 26.

Under the assumption that the hole mobility does not significantly change during the annealing process, an increase in the hole concentration, as seen from Figs. 1 and 2, should result in an increase in the electrical conductivity of the (Ga,Mn)As layer. In fact, such an increase has been observed by several authors.[6,7,9,10] In the present work, the effect of annealing at 250 °C on the conductivity of sample B313 is shown in Fig. 4.

Monitoring the conductivity by an *in situ* measurement for 400 min reveals that the conductivity monotonously rises with a rate that gradually decreases with increasing annealing time. After total annealing times of 30, 60, and 180 min, the annealing process was interrupted for 10 min and the temperature was rapidly lowered to 25 °C in order to probe the RT conductivity (dashed line). During the first 30 min, the RT conductivity increases from 91 to 103 Ω^{-1} cm^{-1}. After annealing for 370 min, the RT conductivity has almost saturated at a value of 116 Ω^{-1} cm^{-1}. According to these values, the conductivity is enhanced by factors of 1.13 and 1.27 upon annealing for 30 and 370 min, respectively. In contrast to Ref. 6, no decrease of the conductivity for annealing times longer than 2 h is observed. Note that the results of our *in situ* measurements are in qualitative agreement with those obtained from much thinner (Ga,Mn)As epilayers (10–100 nm) at lower annealing temperatures ($\leqslant$200 °C).[7,10]

We may now compare the annealing-induced increase of the conductivity with that in hole concentration. From the averaged hole concentrations, derived above from the ECV profiles in Fig. 1, we obtain an increase in hole density by factors of 1.13 ± 0.3 and 1.29 ± 0.4, which are in excellent agreement with the values obtained for the conductivity. Thus, the assumption of at most a small change in hole mobility during annealing is clearly confirmed. From the values of the conductivity and the averaged carrier concentrations, effective hole mobilities of 1.5 ± 0.3 cm^2/Vs are deduced for the as-grown as well as for the annealed samples.

Raman spectra, recorded from sample B313 before and after annealing at 250 °C for 30 and 370 min, are shown in Fig. 5. Whereas a strong increase in the hole concentration within the first 30 min of annealing can be deduced, the Raman spectrum recorded from the 370-min-annealed sample does not significantly differ from that of the 30-min-annealed sample. This is in agreement with the ECV profiles in Fig. 1, which reveal that near the sample surface the hole density is only slightly enhanced by annealing for more than 30 min. For the interpretation of the Raman spectra, one should keep in mind that the Raman signal, as already mentioned above, stems from the near-surface region. The solid lines represent model calculations of the Raman line shapes using a hole mobility of $\mu=1.2$ cm^2/Vs and hole concentrations of 4.3×10^{20} cm^{-3} and 7.8×10^{20} cm^{-3} for the as-grown and the annealed samples, respectively.

According to the relation[4]

$$T_C \propto x \times p^{1/3} \tag{4}$$

between Curie temperature T_C and hole density p, with x denoting the concentration of magnetically active Mn ions on Ga sites, an increase in the hole density should result in an enhancement of the Curie temperature. In fact, such an enhancement is shown by the SQUID magnetization curves in Fig. 6, recorded from sample B313 before and after annealing at 250 °C for 30 and 370 min. Note that the curves are normalized to the values at 5 K, and thus cannot be used to obtain information about the influence of post-growth annealing on the saturation magnetization. We suggest that the extended tails of the magnetization curves arise from the vertical gradient of the hole density p in the (Ga,Mn)As layer. According to Eq. (4), this gradient results in a depth-dependent Curie temperature T_C, and thus the curves in Fig. 6 can be viewed as superpositions of individual magnetization curves. Then, the values of T_C indicated by arrows have to be attributed to the near-surface region, similar to the hole densities obtained from the Raman measurements. Whereas a Curie temperature T_C of 60 ± 5 K is deduced for the as-grown sample, a constant value of 100 ± 5 K is obtained for the two annealed samples, yielding an increase of T_C by a factor of 1.7 ± 0.3. In contrast, an enhancement of T_C by a factor of

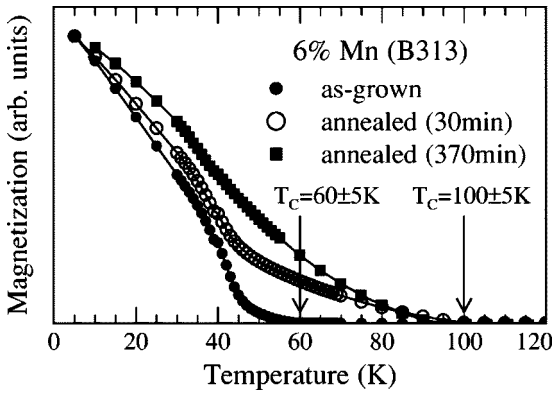

FIG. 6. Normalized magnetization of sample B313 as a function of temperature before and after annealing.

only 1.2 ± 0.1 would have been expected from Eq. (4) and the ECV data measured near the sample surface, yielding an increase of the local hole density by a factor of 1.7 ± 0.5. The discrepancy between the two values may be explained by a reduction of the number of antiferromagnetically ordered Mn atoms[14] during annealing.

The increase in hole density, conductivity, and Curie temperature upon post-growth annealing is commonly explained by the removal of compensating defects in (Ga,Mn)As. The results of ion channeling experiments point to a reduction of Mn interstitials (Mn_I), acting as compensating double donors.[13] Based on the observation of Mn accumulation at the sample surface and on theoretical calculations, this reduction has been traced back to an out-diffusion of Mn_I towards the surface followed by oxidation.[10,12,27] In order to verify the latter suggestion for the thick (Ga,Mn)As layers under study, the Mn depth profiles of the as-grown and the annealed samples were experimentally determined by SIMS measurements recorded from the same sample pieces as used for ECV profiling. The Mn profiles are depicted in Figs. 7 and 8 for B352 and B313, respectively. Whereas Fig. 7 suggests a slight annealing-induced lowering of the Mn fraction in the 240-nm-thick sample, no significant difference between the three profiles of the 1.2-μm-thick sample can be identified in Fig. 8. Inevitably the question arises if an out-

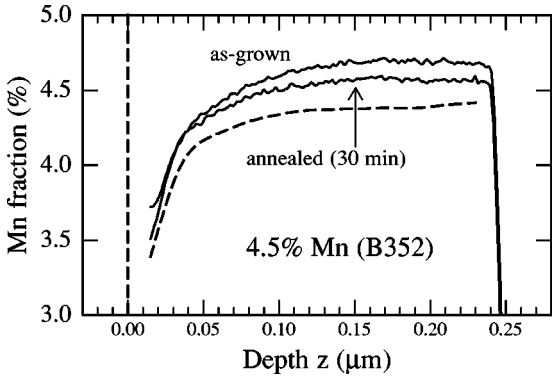

FIG. 7. Mn depth profiles of sample B352 before and after annealing at 250 °C for 30 min measured by SIMS. The dashed line represents the calculated Mn profile of the annealed sample using Eqs. (7) and (8).

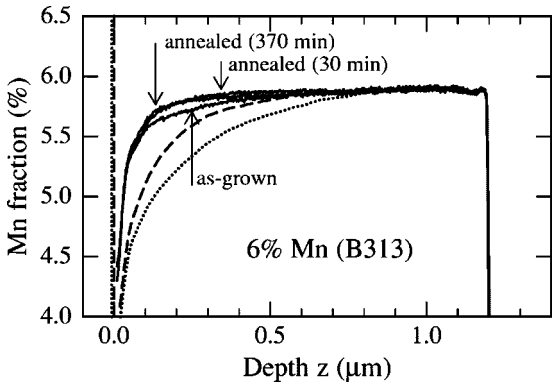

FIG. 8. Mn depth profiles of sample B313 before and after annealing at 250 °C for 30 and 370 min measured by SIMS. The dashed and dotted lines represent the calculated Mn profiles of the 30-min and 370-min-annealed sample, respectively, using Eqs. (7) and (8).

diffusion of Mn_I, necessary to completely account for the observed ECV profiles, would result in a significant and measureable change in the Mn depth profile at all. Therefore, simple considerations are made in the following to estimate the annealing-induced changes in the Mn depth profiles expected for the extreme case that the increase in the hole densities in Figs. 1 and 2 was entirely due to the out-diffusion of Mn_I.

The hole concentration p is given by the density $[Mn_{Ga}]$ of substitutional Mn acceptors (Mn_{Ga}) minus the total density of compensating donors,

$$p = [Mn_{Ga}] - C \times [Mn_I] - d, \tag{5}$$

where $[Mn_I]$ denotes the density of Mn_I and d the density of all other compensating defects. Note that the terms in Eq. (5) are local quantities which may in general vary with depth within the sample. The factor C accounts for the fraction of Mn_I acting as donors as well as for the corresponding valency (2 for double donors). Therefore, the inequality $C \leqslant 2$ holds, where the sign of equality applies for the case that all Mn_I act as double donors. The total density [Mn] of Mn atoms is given by

$$[Mn] = [Mn_{Ga}] + [Mn_I] + [Mn_{ia}], \tag{6}$$

with $[Mn_{ia}]$ denoting the density of electrically inactive Mn atoms. Let us now consider the hypothetical case that the increase in p, revealed by ECV profiling, is solely due to out-diffusion of Mn_I and that inside the (Ga,Mn)As layer, d, $[Mn_{Ga}]$, and $[Mn_{ia}]$ remain unaffected upon annealing. Then, using Eqs. (5) and (6), the local density $[Mn]_{ann}$ of Mn atoms inside the annealed sample ($z > 0$) is given by

$$[Mn]_{ann} = [Mn]_{ag} - (p_{ann} - p_{ag})/C, \tag{7}$$

where the subscripts "ann" and "ag" stand for annealed and as-grown, respectively. The increase in the Mn concentration on the surface ($z = 0$) due to the accumulation of out-diffused Mn_I can be calculated from the conservation of the total amount of Mn as follows:

$$([\mathrm{Mn}]_{\mathrm{ann}} - [\mathrm{Mn}]_{\mathrm{ag}})_{z=0} \times \delta = \int_0^t dz(p_{\mathrm{ann}} - p_{\mathrm{ag}})/C, \quad (8)$$

where t denotes the thickness of the as-grown (Ga,Mn)As epilayer and δ the thickness of the Mn surface layer, which is of the order of nm.

The dashed and dotted lines in Figs. 7 and 8 represent the calculated Mn profiles for the 30-min and 370-min-annealed samples, respectively, using Eqs. (7) and (8) with $C=2$, and taking into account that a Mn fraction of 1% corresponds to a concentration of Mn atoms of 2.2×10^{20} cm^{-3}. For $[\mathrm{Mn}]_{\mathrm{ag}}$, the experimental SIMS profiles of the as-grown samples were used, while p_{ag} and p_{ann} were taken from Figs. 1 and 2. In the case of sample B352, the calculated $[\mathrm{Mn}]_{\mathrm{ann}}$ curve inside the (Ga,Mn)As layer has qualitatively the same form as the measured Mn profile, but quantitatively the annealing-induced decrease in Mn fraction is about twice as strong. Note that our estimate would yield an even more pronounced reduction of the Mn fraction if a value less than 2 had been used for the factor C. Thus, it seems that in the 240-nm-thick sample, only a small portion of the enhancement in hole density is actually due to $\mathrm{Mn_I}$ out-diffusion. In the case of sample B313, the calculated $[\mathrm{Mn}]_{\mathrm{ann}}$ curves inside the epilayer show a clear deviation from the Mn distribution in the as-grown sample, beginning at a depth of about 0.5–0.7 μm and increasing strongly towards the surface. This behavior is not even qualitatively reflected by the measured Mn profiles. Therefore, we conclude that at least in thick (~1 μm) samples, the observed increase in hole concentration in the bulk is not primarily due to out-diffusion of $\mathrm{Mn_I}$. This finding is in agreement with the low diffusivity of $\mathrm{Mn_I}$ at 250 °C derived in Ref. 10. Moreover, the calculated narrow peaks at the surfaces, arising from the accumulation of out-diffused $\mathrm{Mn_I}$, are not seen in the measured SIMS profiles. Calculation yields $([\mathrm{Mn}]_{\mathrm{ann}}-[\mathrm{Mn}]_{\mathrm{ag}})_{z=0} \geqslant 6\%$ for B352 and $([\mathrm{Mn}]_{\mathrm{ann}} -[\mathrm{Mn}]_{\mathrm{ag}})_{z=0} \geqslant 11\%$ for B313 with $\delta \leqslant 10$ nm. Note, however, that the SIMS data presented in Figs. 7 and 8 may be too rough to resolve an extremely thin Mn-rich oxide layer on the surface, if present.

Our findings discussed above do not contradict the model deduced for much thinner (Ga,Mn)As layers ($\lesssim$100 nm) that out-diffusion of $\mathrm{Mn_I}$ plays a dominant role. In fact, the experimental data available so far suggest that, due to the low diffusivity of $\mathrm{Mn_I}$ at 250 °C, a significant out-diffusion of $\mathrm{Mn_I}$ occurs in the near-surface region, whereas in the bulk, the highly unstable $\mathrm{Mn_I}$ atoms rearrange and form electrically inactive randomly distributed precipitates, as proposed in Ref. 13. Within the framework of our simple considerations above, this means that in the bulk the rise in hole concentration p is mainly due to a local increase of $[\mathrm{Mn_{ia}}]$ and/or $[\mathrm{Mn_{Ga}}]$ at the expense of $[\mathrm{Mn_I}]$. From the ECV profiles in Fig. 1, it follows that this rearrangement of $[\mathrm{Mn_I}]$ does not take place homogeneously throughout the whole (Ga,Mn)As layer, leading to an overall upshift of the hole density, but exhibits a pronounced dependence on sample depth. At present, there is no final explanation for this particular evolution of the carrier depth profile on annealing, which seems to be governed by a diffusion-based mechanism. Further experiments such as depth-resolved investigations on the $\mathrm{Mn_I}$ distribution and theoretical studies have to be performed in the future to clarify this point. We close with a brief discussion of two potential mechanisms.

The first mechanism is based on a weak depth-dependent diffusion of $\mathrm{Mn_I}$ towards the surface associated possibly with a change of lattice site location. Initiated by an out-diffusion of $\mathrm{Mn_I}$ in the near-surface region, $\mathrm{Mn_I}$ atoms deeper in the bulk successively diffuse towards the surface while forming electrically inactive Mn clusters and/or MnAs. Due to the low diffusivity of $\mathrm{Mn_I}$, this process gradually becomes ineffective with increasing sample depth. Thus, depending on the annealing time, different diffusionlike profiles of $\mathrm{Mn_I}$ evolve which result in the hole density profiles shown in Figs. 1 and 2. This explanation also accounts for the fact that, compared to the total amount of Mn inside the (Ga,Mn)As layer, only a negligibly small fraction of Mn effectively migrates out of the bulk.

The second mechanism is more hypothetical and rests upon an assumed out-diffusion of highly mobile, possibly compensating, defects other than $\mathrm{Mn_I}$, acting at least partially as a trigger for the rearrangement of $\mathrm{Mn_I}$. Arsenic located in interstitial positions ($\mathrm{As_I}$) may be a potential candidate for such a defect. Similar to LT GaAs,[28–30] the LT MBE growth of (Ga,Mn)As leads to the incorporation of excess As up to 2%, acting at least partially as compensating donor defects.[3,13] Even though controversially discussed, several authors suggest that in LT GaAs a considerable fraction of the excess As atoms is located in interstitial positions, acting as highly mobile defects, while the rest of the excess As is believed to be in antisite positions ($\mathrm{As_{Ga}}$).[31–33] $\mathrm{As_{Ga}}$ defects are known to remain stable up to 450 °C and are therefore not expected to play a significant role in the physical processes taking place at 250 °C.[34] Whereas a rearrangement of $\mathrm{Mn_I}$ could be revealed in (Ga,Mn)As by combined channeling Rutherford backscattering and by particle- induced x-ray emission experiments,[13] out-diffusion of As is difficult to verify. As atoms, which diffuse from interstitial sites to the sample surface during annealing, efficiently desorb at the surface and are therefore hardly detected by surface-sensitive methods.

IV. SUMMARY

The depth profile of the hole concentration in thick ($\geqslant$200 nm) MBE-grown (Ga,Mn)As layers, measured by ECV profiling, as well as its strong change upon post-growth annealing at 250 °C, has been shown to play a key role in the interpretation of conductivity and magnetization data. The annealing-induced increase in the total hole concentration, derived from ECV profiling, is in excellent quantitative agreement with the change in electrical conductivity measured *in situ* during annealing. The pronounced enhancement of the hole density near the sample surface, confirmed by micro-Raman measurements, is accompanied by a distinct increase of the Curie temperature. The particular evolution of the measured ECV profiles under continued annealing suggests that diffusion processes play a major role in the post-growth annealing of (Ga,Mn)As. From a comparison be-

tween the ECV profiles and the Mn distributions determined by SIMS, it is concluded that, in contrast to thin layers, the increase in hole density upon post-growth annealing in thick ($\sim 1\ \mu$m) samples is not primarily due to out-diffusion of Mn_I. We suppose that a depth-dependent rearrangement of Mn_I in the bulk, initiated by an out-diffusion of Mn_I from the near- surface region, accounts for the change in the hole-density profile. Alternatively, a process based on the out-diffusion of other highly mobile defects, such as As_I, has been tentatively discussed.

ACKNOWLEDGMENTS

The authors acknowledge financial support by the Deutsche Forschungsgemeinschaft, Grant No. DFG Wa 840/4.

*Electronic address: wolfgang.limmer@physik.uni-ulm.de; URL: http://hlpsrv.physik.uni-ulm.de

[1] H. Ohno, Science **281**, 951 (1998).
[2] A. Van Esch, L. Van Bockstal, J. De Boeck, G. Verbanck, A. S. van Steenbergen, P. J. Wellmann, B. Grietens, R. Bogaerts, F. Herlach, and G. Borghs, Phys. Rev. B **56**, 13 103 (1997).
[3] F. Matsukura, H. Ohno, A. Shen, and Y. Sugawara, Phys. Rev. B **57**, R2037 (1998).
[4] T. Dietl, H. Ohno, and F. Matsukura, Phys. Rev. B **63**, 195205 (2001).
[5] K. C. Ku, S. J. Potashnik, R. F. Wang, S. H. Chun, P. Schiffer, N. Samarth, M. J. Seong, A. Mascarenhas, E. Johnston-Halperin, R. C. Myers, A. C. Gossard, and D. D. Awschalom, Appl. Phys. Lett. **82**, 2302 (2003).
[6] S. J. Potashnik, K. C. Ku, S. H. Chun, J. J. Berry, N. Samarth, and P. Schiffer, Appl. Phys. Lett. **79**, 1495 (2001).
[7] K. W. Edmonds, K. Y. Wang, R. P. Campion, A. C. Neumann, N. R. S. Farley, B. L. Gallagher, and C. T. Foxon, Appl. Phys. Lett. **81**, 4991 (2002).
[8] B. S. Sørensen, P. E. Lindelof, J. Sadowski, R. Mathieu, and P. Svedlindh, Appl. Phys. Lett. **82**, 2287 (2003).
[9] W. Limmer, A. Koeder, S. Frank, M. Glunk, W. Schoch, V. Avrutin, K. Zuern, R. Sauer, and A. Waag, Physica E (Amsterdam) **21**, 970 (2004); the conductivity data presented in this paper are incorrect and have to be multiplied by a factor of 1.4.
[10] K. W. Edmonds, P. Bogusławski, K. Y. Wang, R. P. Campion, S. N. Novikov, N. R. S. Farley, B. L. Gallagher, C. T. Foxon, M. Sawicki, T. Dietl, M. B. Nardelli, and J. Bernholc, Phys. Rev. Lett. **92**, 037201 (2004).
[11] D. Chiba, K. Takamura, F. Matsukura, and H. Ohno, Appl. Phys. Lett. **82**, 3020 (2003).
[12] M. B. Stone, K. C. Ku, S. J. Potashnik, B. L. Sheu, N. Samarth, and P. Schiffer, Appl. Phys. Lett. **83**, 4568 (2003).
[13] K. M. Yu, W. Walukiewicz, T. Wojtowicz, I. Kuryliszyn, X. Liu, Y. Sasaki, and J. K. Furdyna, Phys. Rev. B **65**, 201303(R) (2002).
[14] J. Blinowski and P. Kacman, Phys. Rev. B **67**, 121204(R) (2003).
[15] A. Koeder, S. Frank, W. Schoch, V. Avrutin, W. Limmer, K. Thonke, R. Sauer, A. Waag, M. Krieger, K. Zuern, P. Ziemann, S. Brotzmann, and H. Bracht, Appl. Phys. Lett. **82**, 3278 (2003).
[16] S. T. B. Goennenwein, T. Graf, T. Wassner, M. S. Brandt, M. Stutzmann, J. B. Philipp, R. Gross, M. Krieger, K. Zürn, P. Ziemann, A. Koeder, S. Frank, W. Schoch, and A. Waag, Appl. Phys. Lett. **82**, 730 (2003).
[17] T. G. Rappoport, P. Redliński, X. Liu, G. Zaránd, J. K. Furdyna, and B. Jankó, Phys. Rev. B **69**, 125213 (2004).
[18] H. Shimizu, T. Hayashi, T. Nishinaga, and M. Tanaka, Appl. Phys. Lett. **74**, 398 (1999).
[19] P. Thompson, Y. Li, J. J. Zhou, D. L. Sato, L. Flanders, and H. P. Lee, Appl. Phys. Lett. **70**, 1605 (1997).
[20] R. Zhao, M. J. Cich, P. Specht, and E. R. Weber, Appl. Phys. Lett. **80**, 2060 (2002).
[21] G. Dollinger, C. M. Frey, A. Bergmaier, and T. Faestermann, Europhys. Lett. **42**, 25 (1998).
[22] P. Blood, Semicond. Sci. Technol. **1**, 7 (1986).
[23] W. Limmer, M. Glunk, S. Mascheck, A. Koeder, D. Klarer, W. Schoch, K. Thonke, R. Sauer, and A. Waag, Phys. Rev. B **66**, 205209 (2002).
[24] M. J. Seong, S. H. Chun, H. M. Cheong, N. Samarth, and A. Mascarenhas, Phys. Rev. B **66**, 033202 (2002).
[25] E. Fuchs, H. Oppolzer, and H. Rehme, in *Particle Beam Microanalysis* (VCH, Weinheim, 1990).
[26] G. Irmer, M. Wenzel, and J. Monecke, Phys. Rev. B **56**, 9524 (1997), and references therein.
[27] K. W. Edmonds, N. R. S. Farley, R. P. Campion, C. T. Foxon, B. L. Gallagher, T. K. Johal, G. van der Laan, M. MacKenzie, J. N. Chapman, and E. Arenholz, Appl. Phys. Lett. **84**, 4065 (2004).
[28] R. E. Pritchard, S. A. McQuaid, L. Hart, R. C. Newman, J. Mäkinen, H. J. von Bardeleben, and M. Missous, J. Appl. Phys. **78**, 2411 (1995).
[29] X. Liu, A. Prasad, J. Nishio, E. R. Weber, Z. Liliental-Weber, and W. Walukiewicz, Appl. Phys. Lett. **67**, 279 (1995).
[30] S. O'Hagan and M. Missous, J. Appl. Phys. **75**, 7835 (1994).
[31] K. M. Yu, M. Kaminska, and Z. Liliental-Weber, J. Appl. Phys. **72**, 2850 (1992).
[32] N. Hozhabri, S.-H. Lee, and K. Alavi, Appl. Phys. Lett. **66**, 2546 (1995).
[33] R. C. Newman, in *Semiconductors and Semimetals*, edited by E. R. Weber (Academic, New York, 1993), Vol. 38, p. 169.
[34] D. E. Bliss, W. Walukiewicz, J. W. Ager III, E. E. Haller, K. T. Chan, and S. Tanigawa, J. Appl. Phys. **71**, 1699 (1992).